Atomic-force-microscope-compatible near-field scanning microwave microscope with separated excitation and sensing probes

K. Lai, M. B. Ji, N. Leindecker, M. A. Kelly, and Z. X. Shen
Department of Applied Physics, Stanford University, Stanford, California 94305
and Geballe Laboratory for Advanced Materials, Stanford University, Stanford, California 94305

(Received 29 January 2007; accepted 13 May 2007; published online 7 June 2007)

We present the design and experimental results of a near-field scanning microwave microscope working at a frequency of 1 GHz. Our microscope is unique in that the sensing probe is separated from the excitation electrode to significantly suppress the common-mode signal. Coplanar waveguides were patterned onto a silicon nitride cantilever interchangeable with atomic force microscope tips, which are robust for high speed scanning. In the contact mode that we are currently using, the numerical analysis shows that contrast comes from both the variation in local dielectric properties and the sample topography. Our microscope demonstrates the ability to achieve high resolution microwave images on buried structures, as well as nanoparticles, nanowires, and biological samples. © *2007 American Institute of Physics.* [DOI: 10.1063/1.2746768]

I. INTRODUCTION

Much of our understanding of the physical properties of a material comes from its interaction with electromagnetic waves. In the far-field radiation region, the measured electrodynamic property is averaged over a length scale in the order of the wavelength (λ), which limits the spatial resolving power to $\sim\lambda/2$, known as the Abbe barrier. In the near-field region with D (dimension of the source) and r (source-sample distance) much smaller than λ, however, the time-oscillating electric and magnetic fields strongly depend on the surrounding materials and contain information of the local sample properties. Combined with serial pixel-to-pixel data acquisition techniques, the spatial resolution of scanning near-field microscopy[1] is then set by the spatial extent of these evanescent fields, rather than the free-space wavelength.

After the original proposal by Synge,[2] near-field microscopy was first demonstrated at microwave frequencies[3] and then extended to the far infrared, infrared, and visible regimes.[1] The past decade has seen renewed effort in the microwave regime to develop a near-field scanning microwave microscope (NSMM) as a scientifically useful instrument.[1,4–6] A NSMM should in principle allow one to directly probe the local radiofrequency (rf) electrodynamic properties, e.g., the surface impedance (Z_S), the complex dielectric permittivity (ε), and permeability (μ).[5] Such a unique feature can be utilized to study both fundamental physical processes, such as classical and quantum phase transitions, and applied science, such as the electrical properties of biological tissues and biopolymers at the microscopic level. On the practical side, state-of-the-art microelectronics and telecommunication devices all operate at gigahertz frequencies, creating huge practical interest in understanding material properties in the microwave regime. Finally, compared to the atomic force microscope (AFM) and scanning tunneling microscope (STM), the long-range electrostaticlike force involved in the NSMM relieves the stringent requirement of proximal probes, thus enabling high-speed, noncontact, and nondestructive measurements.[1,4–6]

The earliest demonstration of the NSMM utilized microwave cavities with a small aperture.[3,7] This geometry suffers strong attenuation because a small aperture is effectively a waveguide working beyond the cutoff condition. The cutoff problem was circumvented by a second design of NSMM based on transmission lines.[8,9] Further improvements incorporated a resonant structure at the probe end of the transmission line.[10] Monitoring the change of resonant frequency and quality factor (Q), several groups have demonstrated different designs of resonant NSMMs with very high sensitivity and spatial resolution.[10–14]

Despite the encouraging progress in NSMMs, several limitations exist in current designs.[15] First, for the single transmission line probe, either resonant or nonresonant, the excitation and the sensing unit share the same electrode. The voltage level in the signal line, which is termed here the common-mode signal, is inevitably high, resulting in large shot noise. Second, in several designs with a feedback mechanism,[4] the reflected wave is used for both detection and tip-sample distance control; thus no independent signal exists for positioning. Finally, the sensing unit of many resonator-based NSMMs is bulky and the sharp STM-like tips are fragile.[13–15] This leads to slow operation and low bandwidth, compromising the unique nature of long-range force involved in a microwave microscope.

In this article, we present a new design using two transmission lines, one for excitation and the other for sensing. With a proper design, the detector can be "orthogonal" in that the signal is minimized in the absence of a sample. The ultimate goal is to implement a high throughput NSMM with isolated excitation and sensing electrodes, both integrated onto a miniature and flexible tip, while still maintaining high sensitivity and spatial resolution.

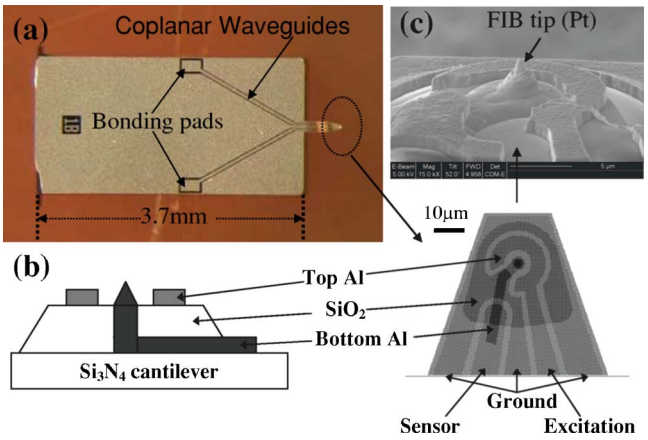

FIG. 1. (Color online) (a) Microfabricated cantilever with coplanar waveguides patterned on the top. The bonding pads and the chip dimension are labeled in the picture. (b) Schematics of the side view (left) and the top view (right) of the cantilever tip. All electrodes are labeled in the figure. (c) Scanning electron microscope (SEM) image of the Pt tip formed by focused-ion beam (FIB) deposition.

II. SYSTEM DESIGN

A. Sensor design

The key feature of our NSMM lies in the design of an orthogonal probe that fulfills the above requirements. We present a detailed design of our sensor built onto an AFM cantilever by standard microfabrication processes, taking advantage of a well developed platform[16,17] that provides the scanning and distance control functions.

Figure 1(a) shows the picture of the overall tip design, which replaces a standard AFM tip assembly, and includes the two transmission lines. The scanning platform we are using is a customized AFM scanner (Pacific Nanotechnology, Inc., Santa Clara, CA). Two 1 μm thick aluminum coplanar waveguides (CPWs) with 50 Ω characteristic impedance are patterned on the bulk part of a silicon chip. One end of each CPW is connected to a bonding pad, and the other end extends all the way to the cantilever beam. The silicon nitride (Si_3N_4) cantilever is 500 μm long and 2 μm thick and is formed by KOH back etch of the Si substrate. We chose Si_3N_4 as the cantilever material because it is less lossy at gigahertz frequencies than Si and more robust than other insulators such as SiO_2.

Figure 1(b) shows the mask design near the end of the cantilever (right) and the schematic of its cross section (left). The layer structure of the sensing unit is shown as follows. On top of the Si_3N_4 cantilever, a short Al strip is deposited as the first metallization. A thick layer of 3 μm plasma enhanced chemical vapor deposited (PECVD) SiO_2 is then deposited at the end of the cantilever beam. A center hole, 3 μm in diameter, is drilled into this oxide layer and back filled with Al. Finally, the top Al layer forms all three (excitation, sensing, and ground) electrodes on the entire chip. Note that while the sensor line for the second Al layer stops at the edge of the SiO_2 coating, the sensing electrode extends all the way to the center hole through the buried Al strip. Such a two-layer implementation proves to be much better than a single-layer structure[15] in common-mode isolation and reduces the noise level significantly. Even with this shielding scheme, however, the direct coupling between the excitation and sensing electrodes is still severe and a common-mode cancellation circuit is needed during the microscope operation.

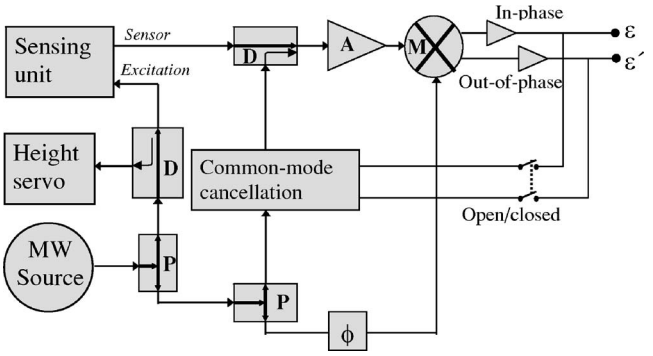

FIG. 2. Block diagram of the microwave circuitry. The microwave components are abbreviated as follows: P—power splitter; D—directional coupler; A—amplifier; M—mixer; and ϕ—phase shifter. Small triangles represent dc amplifiers.

Finally, using a focused-ion beam (FIB) system, we deposited Pt into the center hole for the sensing electrode, as shown in Fig. 1(c). A tip radius of 100 nm is easily achieved in the FIB process, which, in principle, should allow us to reach very high spatial resolution. The drawback is that the FIB process is slow and costly and often compromises the electrical characteristics of the tips. The Pt tip is also quite fragile during the operation and degrades with use.

B. Circuit design

In its essence, our sensing unit measures the transmission from the excitation electrode to the sensor. Signals to and from the probe are routed to 50 Ω matching networks adjacent to the probe. These are optimized at the operating frequency of 1 GHz, but in principle could be broadband transformers. We emphasize that, unlike many existing NSMMs that primarily utilize the frequency shift and change of the Q factor for the measurement,[1,4,6] the electronics here measures the in-phase and out-of-phase components of the sensed signal to determine the complex impedance of the sample.

The microwave circuit diagram is shown in Fig. 2. As mentioned above, due to the incomplete shielding between the excitation and the sensing electrodes, a large common-mode component exists in the sensor signal even in the absence of a sample. To avoid saturating the rf amplifier, the common-mode signal is nulled by injecting a properly phase-shifted and attenuated signal from the generator. In the closed-loop condition, feedback from the output channels can adjust the attenuation in the cancellation unit to correct small drifts of the null signal during scanning. After the cancellation, the detected signal is amplified and demodulated in a quadrature mixer. The in-phase and out-of-phase signals are then amplified and recorded during the AFM scan. After proper calibration in both phase and amplitude, these two output channels manifest the real and imaginary parts of the complex dielectric constant of the sample.

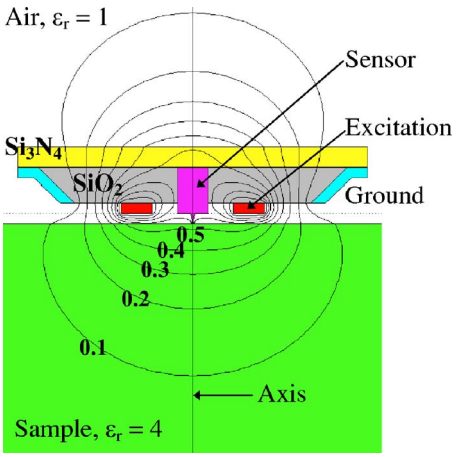

FIG. 3. (Color online) FEMLAB results of the equipotential contour when a sample with $\varepsilon_r=4$ is in contact with the Pt tip. The 2D axisymmetric electrostatic model was used for the simulation, and the excitation voltage is set to 1 V.

One advantage of having two electrodes in the sensing unit is that other signals like the reflection from either electrode can be utilized for the tip-sample distance control. As shown in Fig. 2, the reflected signal from the excitation electrode is collected and detected by the height servo circuit. The output of this circuit serves as the feedback signal that regulates the z piezo in the AFM. Due to the large size ($\sim$20 μm in diameter) of the excitation ring, one measures the averaged reflection over this larger area instead of following every detail of the sample topography. Provided that the electrical property does not change dramatically in the large scale, such servo should be able to keep a constant tip height above the sample. Most data in this article were taken in contact mode with no feedback control, and we are making effort to implement a reliable height servo for noncontact mode.

III. NUMERICAL ANALYSIS

An attractive feature of NSMMs is the ability to image material properties in a quantitative manner.[5] This is largely due to the relatively simple physics when matter interacts with electromagnetic waves in the microwave regime. In our case, since all relevant dimensions are much smaller than the free-space wavelength (30 cm) at the working frequency, the wave nature in the near zone can be ignored and the electrostatic approximation applies.

The finite element analysis (FEA) was performed by using the linear electrostatic model in a software package FEMLAB.[18] As can be seen in Fig. 1, the sensing unit at the end of the cantilever is approximately axisymmetric in shape. As a result, a two dimensional (2D) axisymmetric model was used in most cases to avoid the slow calculation speed and large errors of a large three dimensional (3D) mesh. We believe that the 2D approximation captures the essential physics of the near-field interaction between the sensing unit and the sample.

Figure 3 shows the FEMLAB results of the equipotential contours close to the sensing unit for the FIB tip.[19] The sharp Pt tip is in contact with a sample having a relative dielectric constant (ε_r) of 4. The dimensions in this model are taken from the scanning electron microscope (SEM) image [Fig. 1(c)] of the microfabricated cantilever. For simulation purposes, the Pt tip is assumed to be 1 μm tall with 50 nm radius in the apex. The boundary condition is chosen so that the regions far away from the system (40 μm) are grounded. The excitation voltage is set to 1 V and the shield is grounded.

Figure 4(a) shows the change of the tip voltage in the presence of a sample, $\Delta V_{\text{tip}}=V_{\text{tip}}(\varepsilon_r)-V_0$, where V_0 is the tip voltage for $\varepsilon_r=1$ (air). When the tip scans over a flat sample with regions having different dielectric properties, as shown schematically in the inset of Fig. 4(a), this electrical response provides contrast in the output of the microwave microscope. Practically, the electrical signal is generally much smaller because the contrast only comes from local dielectric variation within a thin layer of the sample.

An important feature of the current design is that the tip signal is sensitive to the sample topography, as well as its electrical properties. A quantitative understanding of the topographical response is shown as the approaching curve in Fig. 4(b) when the tip approaches the sample with $\varepsilon_r=4$. Here the tip signal, $\Delta V_{\text{tip}}=V_{\text{tip}}(d)-V_0$, is plotted as a function of the spacing d between the excitation electrode and the sample. For our tip geometry, much of the signal appearing on the tip electrode comes from the capacitive coupling between the tip and excitation electrodes, rather than the tip-sample coupling. A sample underneath the sensor acts as a partial shield to the tip-excitation capacitance, resulting in a negative approaching curve. When the tip scans over the rough sample surface in a contact mode, as shown in the inset of Fig. 4(b), the entire sensing unit follows the topography and the signal moves up and down in the approaching curve, resulting in contrast in the microscope output.[20]

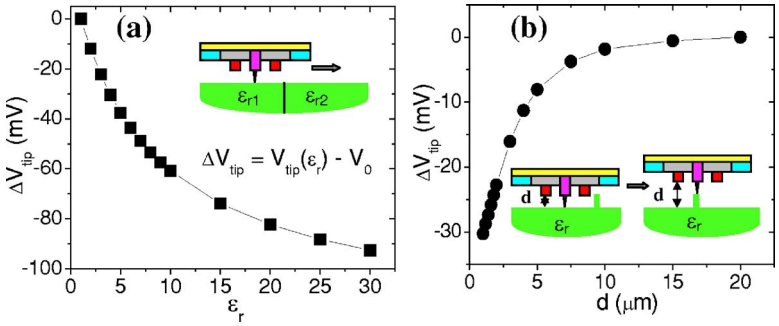

FIG. 4. (Color online) (a) FEMLAB results of the electrical response $V_{\text{tip}}=V_{\text{tip}}(\varepsilon_r)-V_0$ as a function of the sample dielectric constant. This response provides the electrical contrast for a flat surface as shown in the inset. (b) Simulation results of the tip signal when approaching an $\varepsilon_r=4$ sample. Here the spacing is measured from the excitation electrode. The inset shows how topographical contrast occurs in the contact mode.

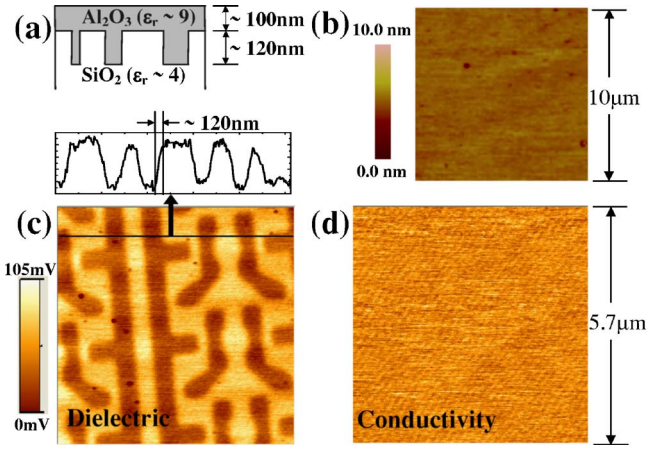

FIG. 5. (Color online) (a) Sample structure—a layer of Al_2O_3 is sputtered onto a SiO_2 sample and then the surface is polished. (b) AFM image of the flat surface. [(c) and (d)] NSMM images from the two output channels in an area of 5.7×5.7 μm^2. Contrast only appears in the dielectric channel and vanishes in the conductivity channel. A line cut of the dielectric channel is also shown, and the spatial resolution of the microscope is about 120 nm.

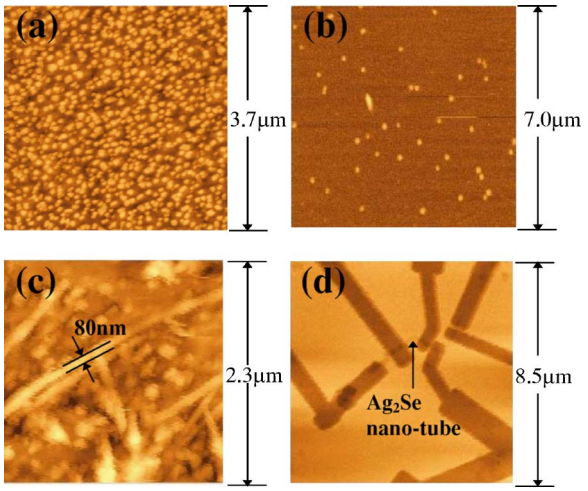

FIG. 6. (Color online) Microwave images convolving both topographical and electrical information. (a) $Pb(Zr,Ti)O_3$ nanoparticles, (b) Au nanoparticles, (c) V_2O_5 nanoribbons, and (d) Ag_2Se nanotubes.

IV. EXPERIMENTAL RESULTS AND DISCUSSIONS

A. Electrical contrast

Due to the long-range electromagnetic interaction between microwave and matter, electrical contrast can be obtained even for flat samples with dielectric variations. This is particularly useful for imaging buried structures in the microelectronic integrated circuits, as well as studying electronic phase transition in fundamental physics.

Figure 5 demonstrates the subsurface imaging ability of our designed NSMM. To avoid the entanglement of electrical and topographical signals, we prepared a smooth sample [Fig. 5(a)] with subsurface dielectric contrast as follows. The patterns with 120 nm depth, as seen in Fig. 5(c), are defined in the thick SiO_2 layer on top of a silicon wafer. A layer of Al_2O_3 is then sputtered onto the device and surface polished. For a consistency check for the smoothness of the surface, the topography is measured by a calibrated Digital Instruments Multimode AFM (Veeco Metrology, Inc., Santa Barbara, CA), as shown in Fig. 5(b). After the polishing, the surface is still fully covered by Al_2O_3, as confirmed by x-ray photoemission spectroscopy. Microwave images from the two output channels are shown in Figs. 5(c) and 5(d). As expected, after properly adjusting the phase ϕ (see Fig. 2), contrast in the conductivity plot vanishes, while the subsurface dielectric contrast is clearly observed. The contrast signal, about 60 mV for this particular sample, can be obtained by taking an arbitrary line cut in Fig. 5(c). A spatial resolution ~120 nm, consistent with the tip diameter, is also extracted from the rising/falling edge across the subsurface boundary of two distinct materials. Detailed quantitative results, e.g., the frequency and amplitude responses, are beyond the scope of this article and will be shown in subsequent publications.

B. Combined topographical and electrical contrast

Many practical applications of the NSMM inevitably involve measuring samples with considerable surface topography. As shown in the numerical analysis, their near-field microwave images will convolve both topographical and electrical information. Proper design of the tip structure and the inclusion of a height control mechanism should, in principle, separate the two contrasts by maximizing one over another. For the current design, the microwave images provides important semiquantitative information on the material properties since the sample topography can be easily obtained by other methods such as SEM, AFM, or simply conventional light microscopy.

Figure 6 shows a collection of the NSMM images for nanoparticles and nanowires. To demonstrate the resolving power to nanometer-size particles, samples with $Pb(Zr,Ti)O_3$ [Fig. 6(a)] or Au nanoparticles [Fig. 6(b)] were prepared and imaged. Particles with size less than 100 nm can be well resolved in the images. For imaging of one dimensional (1D) structures, the microwave images of V_2O_5 nanoribbons grown on Au particles and Ag_2Se nanotubes with contact fingers are shown in Figs. 6(c) and 6(d), respectively. The data again manifest very high resolving power such that wires with a diameter of 80–100 nm are clearly seen in the images. We emphasize that, unlike conventional AFMs, no laser feedback is needed for the operation of the microwave microscope to probe these nanoscale objects.

NSMM techniques are especially attractive for biological applications because of their sensitivity to water and mineral content.[1,6,17,21] Figure 7 shows the microwave images of the antennal lobe and compound eyes of the fruit fly *Drosophila*.[22] Transmission electron microscope (TEM) and light microscope images of similar samples are shown in the insets for comparison. Our microscope is capable of resolving the same features, e.g., the cell and synaptic structures[22] in (a) and (b) and the ommatidial clusters[15,22] in (c) and (d), as other imaging instruments. We are currently trying to apply the technique to quantitative biological measurements.

CONCLUSION

We have demonstrated the design and experimental results of a working near-field scanning microwave micro-

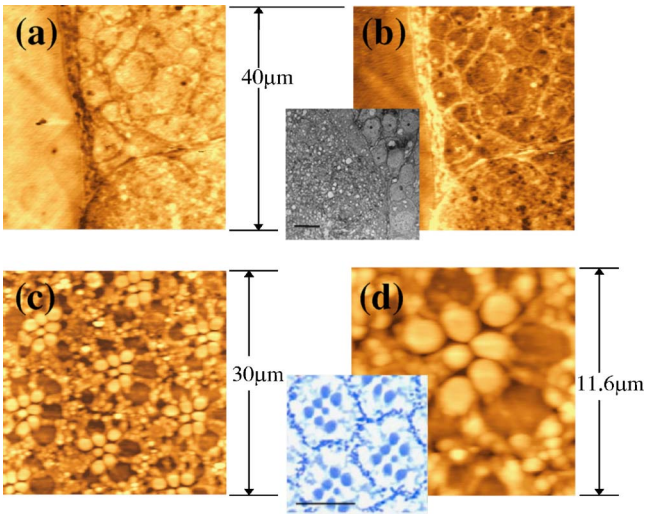

FIG. 7. (Color online) Microwave images of biological samples. (a) In-phase and (b) out-of-phase images of the cell and synaptic structures of an antennal lobe of the *Drosophila* brain. The inset shows the TEM image of a similar sample. (c) The *Drosophila* compound eyes and (d) a zoom-in (11.6×11.6 μm^2) view of the same sample, clearly showing the ommatidial clusters. The inset shows the light microscope image. Both scale bars in the insets are 10 μm.

scope. Microwave CPW transmission lines were patterned onto a Si_3N_4 cantilever interchangeable with AFM tips. A unique feature of our design is that the sensing and excitation electrodes are separated to suppress the common-mode signal. The rf electronics cancels out the remaining common-mode component and amplifies only the change of the tip signal. Numerical analysis using an electrostatic model shows the high sensitivity and spatial resolution of the microscope. The contrast may originate from variation in either sample topography or its electrical properties. Preliminary microwave images on nanoparticles, nanowires, biological samples, and buried insulator structures were obtained by our NSMM. With refined future tip design and reliable height control for the noncontact mode, we believe that this new microwave imager will greatly impact several research fields and find applications in both fundamental physics and applied science.

ACKNOWLEDGMENTS

The research is funded by the seed grant in Center of Probing the Nanoscale (CPN), Stanford University, with partial support from Agilent Technologies, Inc. CPN is an NSF NSEC, NSF Grant No. PHY-0425897. The cantilevers were fabricated by A.M. Fitzgerald and B. Chui in A.M. Fitzgerald & Associates, LLC, San Carlos, CA. The $Pb(Zr,Ti)O_3$ nanoparticle sample was provided by Professor P. McIntyre's group in the Department of Materials Science and Engineering, Stanford University. The samples with Au nanoparticle, V_2O_5 nanoribbons, and Ag_2Se nanotubes were provided by Professor Y. Cui's group in the Department of Materials Science and Engineering, Stanford University. The biological samples were provided by Eric Hoopfer and Chris Winter in Professor L. Luo's group in the Department of Biological Sciences, Stanford University. The authors acknowledge technical support from Agilent Technologies.

[1] For a review of near-field microscopy, see, for example, B. T. Rosner and D. W. van der Weide, Rev. Sci. Instrum. **73**, 2505 (2002).
[2] E. H. Synge, Philos. Mag. **6**, 356 (1928).
[3] Z. Frait, Czech. J. Phys., Sect. A **9**, 403 (1959); R. F. Soohoo, J. Appl. Phys. **33**, 1276 (1962).
[4] S. M. Anlage, D. E. Steinhauer, B. J. Feenstra, C. P. Vlahacos, and F. C. Wellstood, in *Microwave Superconductivity*, edited by H. Weinstock and M. Nisenoff (Kluwer, Amsterdam, 2001), pp. 239–269.
[5] X. D. Xiang and C. Gao, Mater. Charact. **48**, 117 (2002).
[6] S. M. Anlage, V. V. Talanov, and A. R. Schwartz, in *Scanning Probe Microscopy: Electrical and Electromechanical Phenomena at the Nanoscale*, edited by S. V. Kalinin and A. Gruverman (Springer, New York, 2006), pp. 207–245.
[7] E. A. Ash and G. Nichols, Nature (London) **237**, 510 (1972).
[8] C. A. Bryant and J. B. Gunn, Rev. Sci. Instrum. **36**, 1614 (1965).
[9] M. Fee, S. Chu, and T. W. Hansch, Opt. Commun. **69**, 219 (1989).
[10] C. P. Vlahacos, R. C. Black, S. M. Anlage, and F. C. Wellstood, Appl. Phys. Lett. **69**, 3272 (1996).
[11] M. Tabib-Azar, N. S. Shoemaker, and S. Harris, Meas. Sci. Technol. **4**, 583 (1993).
[12] Y. Cho, S. Kazuta, and K. Matsuura, Appl. Phys. Lett. **75**, 2833 (1999).
[13] T. Wei, X. D. Xiang, W. G. Wallace-Freedman, and P. G. Schultz, Appl. Phys. Lett. **68**, 3506 (1996).
[14] C. Gao, T. Wei, F. Duewer, Y. L. Lu, and X. D. Xiang, Appl. Phys. Lett. **71**, 1872 (1997).
[15] Z. Wang, Ph.D. thesis, Stanford University, 2004.
[16] D. W. van der Weide, Appl. Phys. Lett. **70**, 677 (1997).
[17] M. Tabib-Azar and Y. Wang, IEEE Trans. Microwave Theory Tech. **52**, 971 (2004).
[18] FEMLAB, COMSOL, Inc., Palo Alto, CA.
[19] We emphasize that the simulation only considers the sensing unit as an enclosed system. The field distribution is different if the contribution from the rest of the cantilever and the matching network is taken into account, which is beyond the scope of this article and will not be described here.
[20] Since the NSMM is built on an AFM platform, one may attempt to use the *z*-height control from laser feedback to separate the topographical signal from electrical signal. This, however, does not apply because much coupling to the sample actually comes from the excitation ring. While the AFM function can keep the tip in constant height on every detail of the topography, the entire sensing unit still moves up and down with respect to the overall sample surface.
[21] J. Park, S. Hyun, A. Kim, T. Kim, and K. Char, Ultramicroscopy **102**, 101 (2005).
[22] For a summary of the biological samples in this study, refer to Professor Luo's group website http://www.stanford. edu/group/luolab/